Free surface waves induced by vortex shedding in cylinder arrays

Journal of Hydraulic Research, 2016
http://dx.doi.org/10.1080/00221686.2016.1217948

Research paper

Free surface waves induced by vortex shedding in cylinder arrays

DANIELE P. VIERO, Research Engineer, *Department of Civil, Environmental and Architectural Engineering (ICEA), University of Padova, Padova, Italy*
Email: daniele.viero@unipd.it (author for correspondence)

IRENE PRADELLA, PhD Student, *Department of Civil, Environmental and Architectural Engineering (ICEA), University of Padova, Padova, Italy*
Email: irene.pradella@libero.it

ANDREA DEFINA, Full Professor, *Department of Civil, Environmental and Architectural Engineering (ICEA), University of Padova, Padova, Italy*
Email: andrea.defina@dicea.unipd.it

ABSTRACT
The paper presents and discusses the results of an accurate and extensive experimental investigation on the waves that originate when an array of cylinders is placed in an otherwise uniform open channel flow. The study was originally aimed at providing new and more accurate data to calibrate and validate a theoretical model recently proposed in the literature. However, two interesting characteristics of the phenomenon at hand, never reported in the literature, also emerged from the experimental study, i.e. (i) the wave produced by the cylinders is actually a metachronal wave rather than a pure transverse seiche; (ii) two different resonant conditions exist for each single wave mode, i.e. two typical Strouhal numbers characterize the resonance frequency of vortex shedding from the cylinders in an array. Evidence of the metachronal wave, as well as some preliminary data on the longitudinal component of this wave, are given in the paper. Also, the double resonance condition is experimentally demonstrated and discussed.

Keywords: Experimental study; metachronal wave; open channel flow; resonance frequency; standing waves; transverse seiche; vortex shedding

1 Introduction

This investigation originates from a recent work by Defina and Pradella (2014) who proposed a theoretical model to predict the amplitude of the transverse seiche wave that originates when an array of cylinders is placed in an otherwise uniform open channel flow. The transverse standing wave is produced by the periodic lift force associated with vortex shedding behind each cylinder of the array, and the wave amplitude attains a maximum when the vortex shedding frequency matches the natural frequency of the channel (e.g. Zima & Ackermann, 2002). To predict the oscillation amplitude Defina and Pradella (2014) proposed a model based on the analytical solution of the linearized shallow water equations in which the force supplied by the cylinders is replaced by an equivalent, periodic shear stress acting in the transverse direction. The model prediction was compared to experimental data available in the literature, and the comparison was found encouraging but not fully satisfactory since it exhibits a large scatter about the perfect agreement line (Defina & Pradella, 2014, fig. 5). The results reported and discussed in the above work emphasize the need for further specific and accurate experimental investigations aimed at highlighting and distinguishing the different phenomena and interferences that affect the amplitude of the transverse seiche.

The present paper reports and discusses the results of an extensive experimental investigation aimed at (i) accurately measuring the seiche amplitude at different resonant conditions; (ii) understanding the reasons for the large scatter of the results presented in the literature; and (iii) improving our knowledge about the phenomenon which, despite its apparent simplicity, turns out to be very complicated. Before presenting and discussing the experimental findings, we briefly describe the main features of the phenomenon and recall the studies available in the literature.

Received 20 October 2015; accepted 12 July 2016/Currently open for discussion.

ISSN 0022-1686 print/ISSN 1814-2079 online
http://www.tandfonline.com

1.1 *Vortex-induced cross-flow seiching in cylinder arrays*

Consider an array of vertical cylinders placed in an otherwise uniform open channel flow. When the cylinder Reynolds number, R, is in the range of vortex shedding, a cross-flow seiche can be generated due to the periodic lift force associated with vortex shedding (Zima & Ackermann, 2002).

This phenomenon was sometimes observed in real systems, e.g. in canals with bridge piers (Schuster, 1967) and in spillways with openings separated by piers (Hanko, 1967), causing problems related to flow unsteadiness and erosion (Falvey, 2003; Rahmeyer, Robison, & Barfuss, 2010). More often, it was observed in laboratory experiments in which an array of cylinders was used to mimic rigid vegetation (e.g. Peruzzo, Defina, & Nepf, 2012; Zima & Ackermann, 2002, and references therein). The phenomenon shares some similarities with the vortex-induced vibration (VIV); for a review on VIV the reader is referred to Williamson and Govardhan (2004, 2008). Within the VIV framework, one of the most well-known features of the fluid–cylinders interaction is the primary lock-in regime. This occurs when the frequency of vortex shedding, f_v, is close to the natural (or forced) oscillation frequency of the cylinder. In this region, vortex shedding is entrained by the transverse flow and the vortex shedding frequency changes to match the cylinder oscillation frequency.

Oengören and Ziada (1992, 1998) and Ziada and Oengören (1993, 2000) confirmed the qualitative equivalence between VIV and the transverse seiching in open channel flow. They found that (i) a lock-in region straddling the resonance condition also for the case of water waves actually exists; (ii) in this region, vortex shedding is synchronized with the transverse seiching, i.e. vortices shedding from all cylinders, through a feedback mechanism, become correlated and are in phase with each other and with the seiche; (iii) the natural oscillation frequency is accurately predicted by the small-amplitude wave theory; and (iv) the largest amplitude oscillations occur within the lock-in region.

Three typical frequencies characterize the phenomenon. First, the frequency f_S of vortex shedding from an isolated circular cylinder:

$$f_S = \frac{\mathsf{S_t} U}{d} \tag{1}$$

where U is the bulk flow velocity, d is the cylinder diameter, and $\mathsf{S_t}$ is the Strouhal number. The second typical frequency is the natural oscillation frequency of the channel, f_n. As stated above, this frequency is accurately predicted by the small-amplitude wave theory. However, due to the presence of the cylinders, the volume of water per unit volume is smaller than one, and this affects the natural oscillation frequency. To account for the presence of the cylinders, Zhao, Cheng, and Huang (2014) proposed a correction to the standard formula. The corrected formula reads:

$$f_n = \sqrt{(1-s)\frac{gn}{4\pi B}\tanh\frac{\pi h_0 n}{B}} \tag{2}$$

where s is the cross-sectional area of a cylinder per unit horizontal area (i.e. $s = \pi n_c d^2/4$, with n_c being the number of cylinders per unit horizontal area), B is the channel width, h_0 is the mean flow depth, n is the wave mode (i.e. the number of half-wavelengths across the channel), and g is gravity acceleration. The third typical frequency is the actual vortex shedding frequency f_v, which, for steady periodic condition, corresponds to the seiche wave frequency. Vortex shedding frequency can be different from f_S both because of the interaction between the wakes from the upstream cylinders and the boundary layer of the downstream cylinders, and because of the transverse periodic flow induced by the lift force.

When f_S is close to f_n, i.e. within the lock-in region, the actual shedding frequency f_v, through a feedback mechanism, changes to match the natural oscillation frequency. This feedback mechanism also forces vortex shedding from all the cylinders aligned in the transverse direction to be synchronized, i.e. to be correlated and in phase with each other and with the seiche wave. Few studies specifically addressed the issue of transverse seiching produced by an array of vertical cylinders in an open channel flow. Zima and Ackermann (2002), who studied the phenomenon using suitable designed experiments, provided a first, systematic work. They found that the greatest wave amplitude occurs when the frequency ratio f_n/f_S is in the range between 0.7 and 1.3, i.e. close to resonance condition, and measured wave amplitudes as large as 35% of the mean flow depth at resonance. They also proposed an equation to predict the maximum wave amplitude; their equation, rewritten using present notation, reads:

$$\frac{A}{h_0} = 2.255\frac{d}{B} n_c d^2 \mathsf{S_t}^{-2} \tag{3}$$

where A is the wave amplitude (Fig. 1). Ghomeshi, Mortazavi-Dorcheh, and Falconer (2007) and Jafari, Ghomeshi, Bina, and Kashefipour (2010) presented extensive experimental investigations and discussed the results within the framework of dimensional analysis. In both these works simple equations relating the seiche wave amplitude to a set of dimensionless parameters are proposed and assessed through a linear regression on experimental data. However, Defina and Pradella (2014) showed that the regression equations proposed by Ghomeshi et al. (2007) do not fit with experimental data collected by Jafari et al. (2010) and vice versa. A recent, experimental contribution to the issue is provided by Zhao et al. (2014) who experimentally verified Eq. (2) to predict the natural oscillation frequency. They also found that a longitudinal wave was always present when transverse standing waves could be observed for different wave modes. Although observed and mentioned in the literature, the presence of longitudinal waves received little attention in previous studies on transverse seiching.

2 Materials and methods

As stated above, the main purpose of the present experimental investigation was to accurately measure the amplitude of the transverse oscillations in order to test, and possibly to improve the model proposed by Defina and Pradella (2014). The experiments also served to improve our knowledge about this phenomenon and to figure out the reasons why the scatter of the experimental points around the theoretical prediction is so significantly high, regardless of the theoretical formulation.

2.1 *The experimental set-up and procedure*

The experiments are carried out in two tilting flumes. The small flume has a width of 30 cm and length of 6 m, the large flume has a width of 38.4 cm and length of 20 m. In both flumes, water is recirculated via a constant head tank that maintains steady flow conditions, and the flow rate is measured by a magnetic flowmeter (accuracy of about 0.2%). A downstream weir can adjust water depth in the small flume; a vertical sluice gate is used to adjust water depth in the large flume. Data from the two flumes provide a first insight into the possible role played by the channel width. The cylinders used in the experiments are plastic dowels with a diameter of 20 mm, fitted into holes drilled into an overtopping board constructed with longitudinal bars as shown in Fig. 1.

The length of the reach occupied by the cylinder is $L = 1.0$ m in the small flume ($L/B = 3.3$), and $L = 6$ m in the large flume ($L/B = 15.6$). For both flumes, the ratio L/B is large enough (i.e. $L/B > 2$ as suggested by Zima & Ackermann, 2002) to prevent effects on the potential for wave generation or seiching. In the large flume six different arrays were constructed with three cylinder densities (i.e., $n_c = 86.6\,\mathrm{m}^{-2}$, $n_c = 43.3\,\mathrm{m}^{-2}$, $n_c = 28.9\,\mathrm{m}^{-2}$, with n_c the number of cylinders per unit horizontal area) and two arrangements, namely in-line and staggered. The different cylinder densities are achieved by changing only the spacing between cylinders in the longitudinal direction; for the above three densities, relative cylinder spacing, P/d, is 6, 12, 18, with P the longitudinal distance between two cylinders (Fig. 2). One cylinder configuration, arranged in a staggered pattern with $n_c = 83.3\,\mathrm{m}^{-2}$, was used in the small flume (Fig. 2). Experimental conditions are summarized in Table 1.

We used ultrasonic sensors to measure free surface oscillation (accuracy of about 0.13 mm). In order to avoid interferences with the vertical walls, the ultrasonic sensors measured the water level at a distance of 30 mm from the wall. We performed some preliminary measurements and found that the instantaneous free surface profile in the transverse direction, y, is well approximated by $\eta(y) = a\cos(my)$, with η the free surface elevation relative to the mean water depth, a the instantaneous semi-amplitude of the transverse wave (see Fig. 1), and m the wavenumber (see also Zhao et al., 2014). We used this approximation to extrapolate water elevation at the wall. It is worth noting that, for mode one waves, the correction factor, i.e. the ratio between the water elevation, η, at the wall and that measured 30 mm from the wall is just greater than one, being 1.05 for the small flume and 1.03 for the large flume.

We also performed some preliminary experiments, in the large flume, to investigate the impact of non-uniform flow conditions on the wave amplitude. We varied the bottom slope in the range 0.0005–0.007 and adjusted the downstream gate to produce a constant water depth at the middle section (S_2 in Fig. 1). The results of these experiments, that included uniform flow conditions along the cylinder array, showed that differences in the relative wave amplitude are negligibly small ($\pm 5\%$) and did not show any evident trend. Accordingly, all experiments were performed with a constant bottom slope of 0.004. With this slope the flow is uniform along the reach with the cylinders when flow rate is $12\,\mathrm{l\,s}^{-1}$, water depth is 0.19 m (i.e. $U = 0.16\,\mathrm{m\,s}^{-1}$), and for the densest cylinder array.

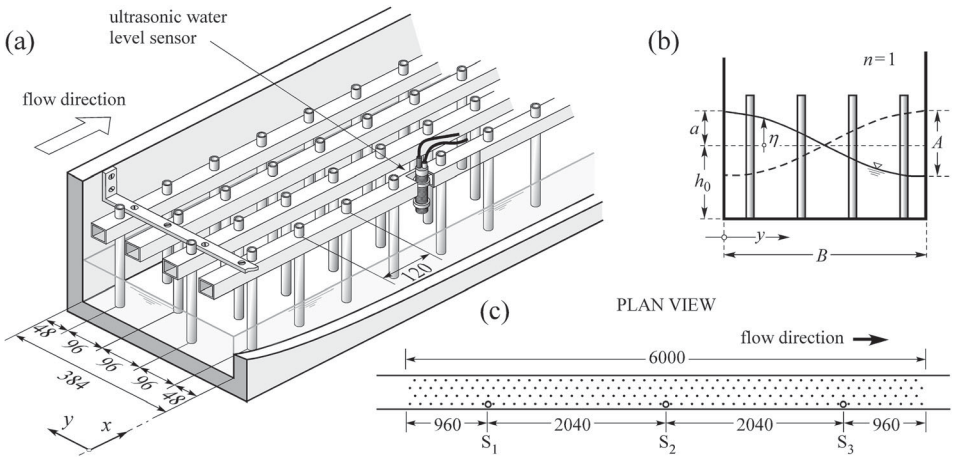

Figure 1 Cutaway view (a), vertical cross section (b), and plan view (c) of the experimental set-up for the large flume (lengths are in mm). S_1, S_2, and S_3 (panel c) denote the positions of the ultrasonic water level sensors. Experimental set-up for the small flume is similar, with the overtopping board constructed with three longitudinal bars

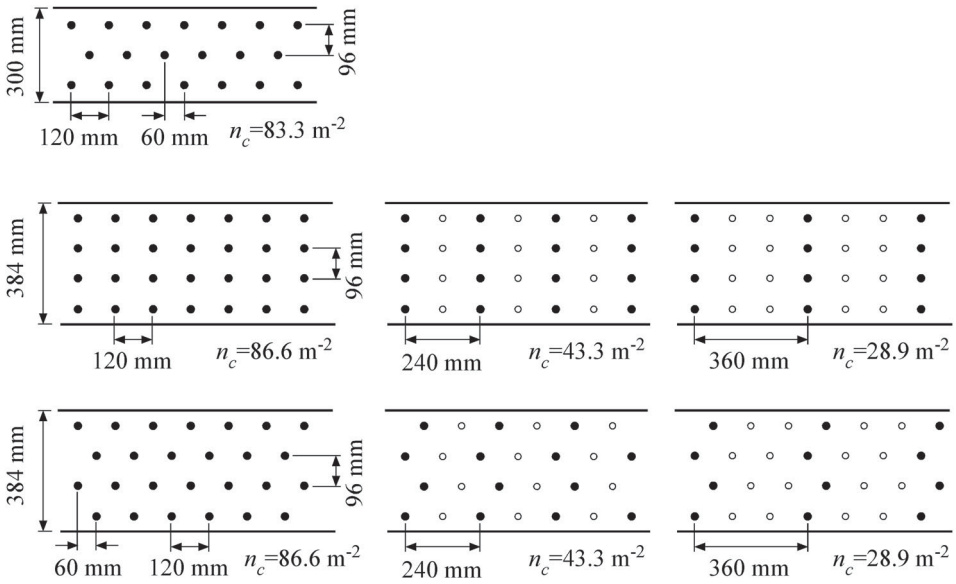

Figure 2 Cylinder configurations used in the experiments performed in the small ($B = 300$ mm) and large flumes ($B = 384$ mm)

Table 1 Summary of present experimental conditions. Symbols are: L is the length of the reach with the cylinders, n_c is the number of cylinders per unit area, $\mathsf{F}_0 = U(gh_0)^{-1/2}$ is the Froude number, and $\mathsf{R} = DU\nu^{-1}$ is the Reynolds number

	Small flume	Large flume
B (m)	0.30	0.384
L (m)	1.0	6.0
L/B	3.3	15.6
h_0 (m)	0.08–0.20	0.10–0.32
U (m s^{-1})	0.15–0.20	0.15–0.20
n_c (m^{-2})	83.3	28.9, 43.3, 86.6
F_0	0.14–0.19	0.10–0.16
R	3115–4030	2260–3970

During each series of the tests, the discharge was held constant while the water depth varied at small steps by adjusting the downstream gate. In order to search for the presence of possible hysteretic behaviours, if any, measurements were performed both by decreasing water depth starting from an initially large water depth, and by increasing water depth starting from an initially small water depth. No hysteresis has ever been detected.

Each series of the test was repeated two or three times by the same or (more frequently) by different operators, showing good repeatability and reproducibility (see e.g. Figs 3 and 5, where different symbols refer to different operators). The study focused on the first wave mode. Only few experiments were extended to include the second wave mode. In our experimental set-up, in fact, the second wave mode occurred at very small flow depth; in these conditions, short irregular waves, produced at the surface by each cylinder, superposed to the free surface oscillation, thus compromising the quality of the recorded signal.

3 Results and discussion

In addition to the collection of accurate wave amplitude data for different cylinder arrangements and flow conditions, some new results, which are discussed in this section, have emerged from the experiments. In particular, we found that the longitudinal wave observed by Zima and Ackermann (2002), Sarkar (2012), and Zhao et al. (2014) always formed in our experiments. We show that this longitudinal wave does not stem from disturbances in the flow field but it is an intrinsic characteristic of the phenomenon at hand. A further interesting finding is that a dual resonance condition (i.e. two different resonant frequencies for the same wave mode) exists, possibly related to the different vortex shedding frequencies of the upstream and inner cylinders of the array.

3.1 *The metachronal wave*

Zima and Ackermann (2002) observed longitudinal progressive waves and beating which superposed to the transverse seiche; they found that these waves could be reduced by placing a fibrous wave-absorbent material at the downstream end of the flume, but they could not be removed. Therefore, they implicitly assumed that the observed progressive longitudinal waves are disturbances triggered by reflection phenomena. Zhao et al. (2014) also reported the persistent presence of longitudinal waves superposing to the transverse seiche. They suggested that the longitudinal waves are disturbances generated downstream of the cylinder array due to the quick velocity slow-down from the reach occupied by the cylinders to the cylinder-free reach. The above authors do not provide any quantitative information about these longitudinal waves, which are likely to affect the transverse oscillation by feeding and extracting momentum from the mean periodic flow within the reach occupied by the cylinders.

In our experiments, we always observed longitudinal waves superposed to the transverse oscillation. Longitudinal waves were always observed to propagate upstream; they have the same frequency as the transverse wave but their wavelength is much greater than that of the transverse wave. Therefore, their celerity turns out to be much faster than that predicted by the linear theory. We then conclude that the observed longitudinal wave is not a disturbance in the flow field. The reason for this longitudinal wave is likely due to a spatially delayed synchronization in the longitudinal direction. The longitudinal synchronization is promoted by the interaction between the wakes from the upstream cylinders and the boundary layer of the downstream cylinders and by the transverse shear stress that arise when the transverse oscillating flow is out of phase. In the absence of longitudinal synchronization, in fact, a longitudinal gradient of the transverse velocity component arises which leads to the inception of transverse shear stresses, which, in turn, act to synchronize vortex shedding in the longitudinal direction. However, such a mechanism is not supposed to ensure perfect synchronization, and could well lead to a phase delaying of the transverse, standing wave in the longitudinal direction.

In our experiments, the free surface elevation can be well described by:

$$\eta(x,y,t) = a\cos(my)\sin(\omega t + kx + \varphi_0) \tag{4}$$

where $a = A/2$ is the wave semi-amplitude (see Fig. 1), $m = \pi n/B$ is the transverse wavenumber with n being the wave mode and B is the channel width, $\omega = 2\pi f_v$, f_v is the actual vortex shedding frequency, k is the longitudinal wavenumber, and φ_0 is a generic phase shift. Therefore, according to the experimental evidence, the observed transverse oscillation and longitudinal wave turn out to be, respectively, the transverse and longitudinal component of a metachronal wave (Brennen & Winet, 1977) produced by the sequential action of the lift force. The seiche wave referred to in the previous literature is then the component of the metachronal wave in the transverse direction. For this reason, although improperly, the transverse component of the metachronal wave is also referred to here as seiche wave. We used Eq. (4) to fit experimental data and evaluate A, ω and k. Fourier analysis of water elevation data was also performed mainly to detect frequencies other than the main oscillation frequency.

3.2 *The transverse component of the metachronal wave: typical frequencies and the dual resonance condition*

While processing the data measured at the beginning of the experimental period we found that, at resonance, the values for the ratio f_S/f_v all clustered around two specific values, namely $f_S/f_v = 1.0$ and $f_S/f_v = 1.2$–1.4. We found this result quite surprising, especially because we could not recognize any correlation between the selected ratio f_S/f_v and any geometric or flow characteristics. The reason for this strange behaviour was revealed by greatly extending the range of the investigated water depths straddling the first detected resonance condition: two distinct resonance conditions, for the same wave mode, n, coexist. Examples of the relative seiche amplitude A/h_0 as it varies with the reduced velocity are given in Fig. 3. The reduced velocity, U_r, typically used in VIV studies, is based on the first-mode, natural oscillation frequency, f_1 (Eq. (2)) as:

$$\mathsf{U}_\mathsf{r} = \frac{U}{f_1 d} \tag{5}$$

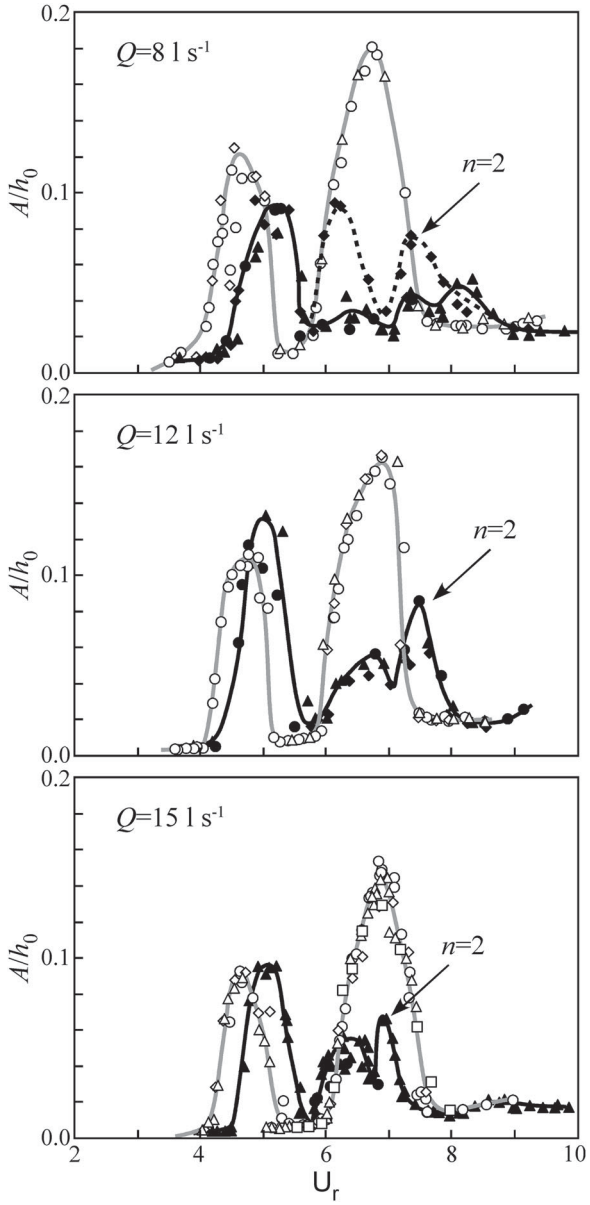

Figure 3 Relative seiche amplitude A/h_0 as a function of the reduced velocity (in-line configuration, large flume). White and black symbols denote $n_c = 86.6\,\mathrm{m}^{-2}$ and $n_c = 43.3\,\mathrm{m}^{-2}$, respectively; the different symbol shapes denote different operators. The leftmost peak corresponds to the primary resonance condition; the third peak when $n_c = 43.3\,\mathrm{m}^{-2}$ corresponds to wave mode $n = 2$. Plotted data are measured by the innermost ultrasonic sensor (denoted by S_2 in Fig. 1)

Figure 3 shows that a first resonance condition is detected when f_S/f_v is close to 1. By progressively reducing the water depth (i.e. by increasing U_r) the relative wave amplitude quickly reduces. By further decreasing the flow depth (i.e. by further increasing U_r), the wave amplitude grows again, producing a second resonance condition characterized by a larger f_S/f_v ratio. For smaller water depths (i.e. larger values of U_r) the seiche definitively vanishes.

It is worth noting that the existence of a dual resonance condition for the case of water waves was never reported in the literature. Within the VIV framework, the existence of more than one Strouhal number triggering resonance is well documented (e.g. Oengören & Ziada, 1992, 1998; Polak & Weaver, 1995; Ziada & Oengören, 2000). However, in VIV studies, the investigated spacing ratios are relatively small (approx. $P/d < 3$) whereas, in the present experiments, as well as in most of experiments on vortex induced surface water waves, the spacing ratio is relatively larger.

Since vortex shedding and lift force are controlled by the specific interaction mechanisms between the wakes from the upstream cylinders and the boundary layer of the downstream cylinders, the results of the above VIV studies can hardly be used in the discussion of the present findings. In addition, in the case of water waves, the strong transverse flow is likely to affect significantly the phenomenon.

Remarkable information is provided by the studies on vortex shedding and resonance mechanisms of two tandem cylinders in cross-flow at large spacing ratios. King and Johns (1976) studied the lateral vibrations of two tandem cylinders in an open channel flow. In their experiments the relative spacing was $P/d = 6.5$, hence comparable to the present spacing when cylinder density is $n_c = 86.6\,\mathrm{m}^{-2}$. When plotting the amplitude of the transverse displacement as a function of the reduced velocity they observed two peaks: the smaller peak occurred at the reduced velocity $U_r = 5.5$ ($S_t \cong 0.182$, which corresponds to the Strouhal number for an isolated cylinder); the larger peak occurred at the reduced velocity $U_r = 7.5$ ($S_t \cong 0.13$). This result was confirmed by Alam and Zhou (2008) who found one peak at $S_t = 0.196$ (close to $S_t = 0.198$ measured for an isolated cylinder) and one peak at $S_t = 0.12$, when the spacing ratio was $P/d = 6$. Importantly, they also observed that the two frequencies were intermittently the same, or "locked-in", for the upstream and downstream cylinders.

The above studies and findings suggest that the reason for the existence of two Strouhal numbers for an array of cylinders is likely related to the different flow field experienced by the most upstream and by the inner cylinders of the array. Interestingly, the upstream cylinders have a Strouhal number corresponding to that of an isolated cylinder while the inner cylinders have a smaller Strouhal number when spacing is relatively large. Importantly, both upstream and downstream cylinders can force the same shedding frequency for all the cylinders of the array.

In most of our experiments, we recognized two distinct peaks for $n = 1$ and for both the staggered and in-line configurations.

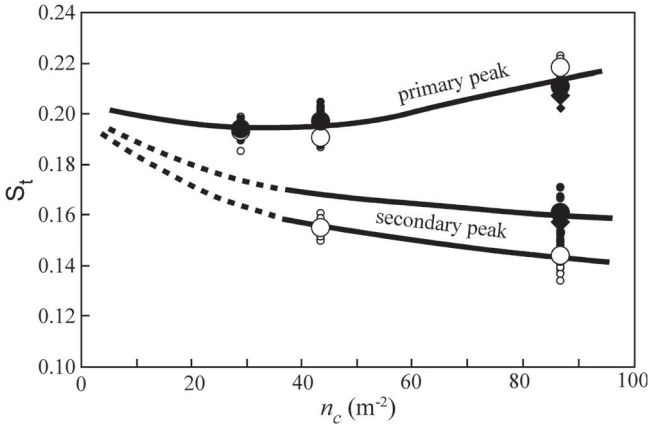

Figure 4 Strouhal number as a function of cylinder density n_c. White and black symbols denote in-line and staggered arrangements, respectively; small circles and diamonds denote measurements taken in the large and small flumes, respectively; large symbols mark the corresponding average values

At resonance, the vortex shedding frequency is assumed to match the seiche frequency (i.e. $f_S = f_n$), and the Strouhal number can be evaluated from Eq. (1) as $S_t = f_S\, d/U$. The first peak has a Strouhal number of approximately $S_{t1} = 0.2$, which is typical of an isolated cylinder for the present range of Reynolds number; this condition is here referred to as primary resonance condition. The second peak corresponds to a Strouhal number approximately in the range $S_{t2} = 0.14$–0.16; we define this condition as secondary resonance condition. Also, hereinafter, we denote with f_{S1} and f_{S2} the Strouhal frequency for S_{t1} and S_{t2}, respectively.

In all experiments with cylinder density $n_c = 86.6\,\mathrm{m}^{-2}$ two clear peaks for $n = 1$ have been detected (white symbols in Fig. 3). In this case the secondary resonance condition have a Strouhal number of approximately $S_{t2} = 0.145$ for the in-line arrangement and $S_{t2} = 0.16$ for the staggered arrangement (Fig. 4). The relative wave amplitude at secondary resonance was always found to be greater than that at the primary resonance condition. In addition, experimental repeatability was very good with minor uncertainties affecting only data pertaining to the primary resonance condition.

Two distinctive peaks for wave mode $n = 1$ were detected also when the cylinder density was $n_c = 43.3\,\mathrm{m}^{-2}$. In this case, the secondary peak is lower, often much lower than the primary peak (full symbols in Fig. 3) and it occurs at a Strouhal number of approximately $S_{t2} = 0.155$ (Fig. 4). Experimental repeatability was not as good as for the densest arrangement; as an example, the upper panel of Fig. 3 shows two relatively different behaviours in the range of reduced velocity pertaining to the first mode, secondary resonance condition and to the second mode, primary resonance condition (i.e. $U_r > \sim 5.8$ when $Q = 81\,\mathrm{s}^{-1}$). For the case $n_c = 28.9\,\mathrm{m}^{-2}$, only the primary resonance condition could be observed for both in-line and staggered arrangement.

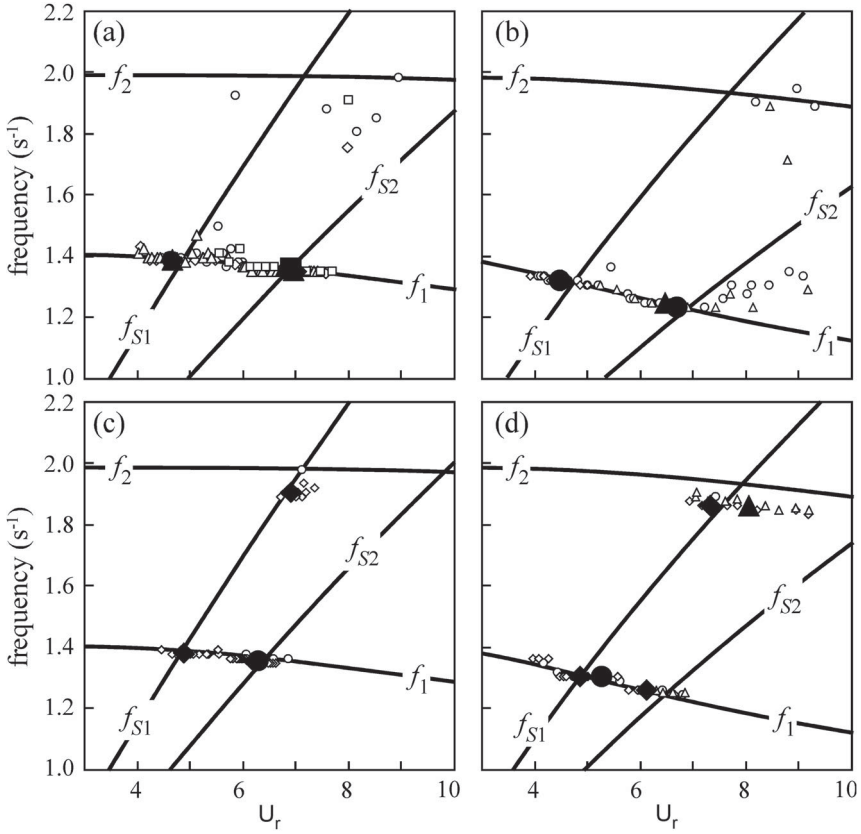

Figure 5 Four typical frequencies f_{S1}, f_{S2}, f_1, f_2, as a function of the reduced velocity for the large flume and in-line arrangement: (a) $Q = 15\,\mathrm{l\,s^{-1}}$, $n_c = 86.6\,\mathrm{m^{-2}}$; (b) $Q = 8\,\mathrm{l\,s^{-1}}$, $n_c = 86.6\,\mathrm{m^{-2}}$; (c) $Q = 15\,\mathrm{l\,s^{-1}}$, $n_c = 43.3\,\mathrm{m^{-2}}$; (d) $Q = 8\,\mathrm{l\,s^{-1}}$, $n_c = 43.3\,\mathrm{m^{-2}}$. White symbols denote frequencies corresponding to the peak of the Fourier spectrum; the different symbols shapes denote different operators. Black symbols denote conditions (U_r, f_v) at the A/h_0 peaks. Plotted data are measured by the innermost ultrasonic sensor (denoted by S_2 in Fig. 1)

The overall behaviour is therefore consistent with the idea that by increasing the spacing between cylinders the interaction between the wakes from the upstream cylinders and the boundary layer of the downstream cylinders weakens, leading to one resonance condition occurring at a Strouhal number corresponding to that of an isolated cylinder.

For the highest cylinder density and for flow conditions such that S_{t1} should excite wave mode $n = 2$, this wave mode was never observed while a regular, approximately sinusoidal signal was measured with a frequency corresponding to the natural frequency of the channel for wave mode $n = 1$. Also, Fourier analysis showed a secondary peak at the frequency f_{S1}, but this peak is by far smaller than that establishing at the frequency f_{S2} thus confirming that the contribution of the second mode is negligibly small. This behaviour can be better described with the aid of Fig. 5 showing the shedding frequencies f_{S1} and f_{S2}, and the natural oscillation frequencies f_1 and f_2 for the first and second mode, respectively, as they vary with the reduced velocity. Intersections between the curves indicate the different resonance conditions. When both flow rate and cylinder density are large (Fig. 5a) the resonance conditions $f_2 = f_{S1}$ and $f_1 = f_{S2}$ occur at approximately the same value of U_r. In this case, the first mode, secondary resonance oscillation, suppresses the second mode, primary resonance. Interestingly, the same suppression occurs when flow rate is moderately small (Fig. 5b) although $f_1 = f_{S2}$ occurs at $U_r = 6.9$ whereas $f_2 = f_{S1}$ occurs at $U_r = 7.9$, i.e. the two resonance conditions do not overlap. Possibly, when the cylinder density is high, upstream cylinders cannot force the same shedding frequency (i.e. $f_2 = f_{S1}$) to the downstream cylinders, and vortex shedding does not synchronize throughout the array.

Conversely, when the cylinder density is small (panels c and d of Fig. 5), the second mode, primary resonance oscillation is always observed, even at large flow rate when the resonance conditions $f_2 = f_{S1}$ and $f_1 = f_{S2}$ occur at approximately the same value of U_r. In this case, the wake interaction mechanism promoting the first mode, secondary resonance is not strong enough to suppress the second mode, primary resonance.

The experimental results show that the phenomenon is actually very complex, especially when the cylinder density is small and mechanisms promoting the vortex shedding synchronization over the whole array at the secondary resonance condition are not effective, so that the measured data are somewhat uncertain. In addition, because of the limitations imposed by the experimental set-up, we could not investigate when, and the reason why, the secondary resonance condition prevails over the second mode, primary resonance. The issue definitely deserves further, specific, investigation.

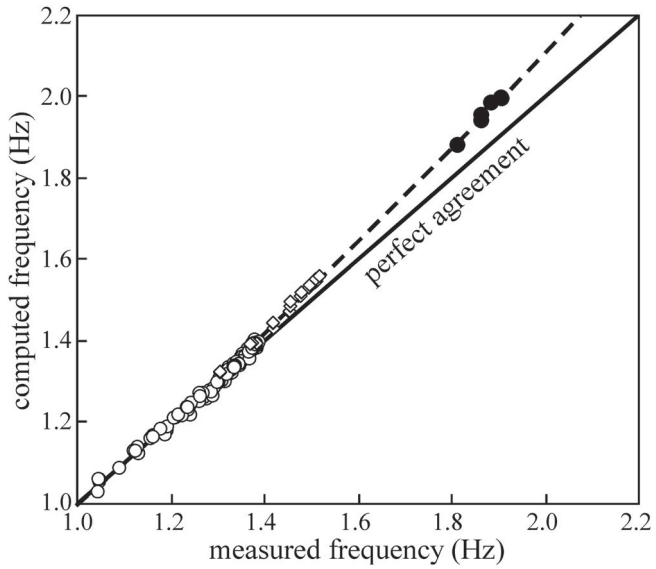

Figure 6 Comparison between measured and computed wave frequency at resonance. White symbols denote first mode values for the large (circles) and small (diamonds) flumes; black symbols denote frequency of the second wave mode

We also compared measured frequency against natural oscillation frequency to check the reliability of Eq. (2). Figure 6 shows that, irrespective of the cylinder density and arrangement, flume width, and resonance conditions, Eq. (2) accurately predicts the natural oscillation frequency when frequency is smaller than 1.2–1.4 s^{-1}. With frequency increasing, Eq. (2) over-predicts more and more the actual frequency; for the second wave mode, the computed frequency is approximately 4–5% greater than the measured frequency (see also panels c and d of Fig. 5).

3.3 *The relative wave amplitude*

To predict the oscillation amplitude, Defina and Pradella (2014) proposed a model based on the analytical solution of the linearized shallow water equations in which the force supplied by the cylinders is replaced by an equivalent, periodic shear stress acting in the transverse direction. According to the model, the relative wave amplitude at resonance is given by:

$$\frac{A}{h_0} = \frac{A_m}{1 + (A_D/dBn_c)}\mathsf{F}_0 \tag{6}$$

where A_m and A_D are two calibration parameters. To include the energy dissipation due to the turbulent diffusion of momentum, Defina and Pradella (2014) introduced an eddy viscosity coefficient proportional to the flow velocity times B/n as significant length scale (the reader is referred to Defina & Pradella, 2014 for details). By replacing flow velocity with $(gh_0)^{1/2}$ in the definition of the eddy viscosity, the following equation can be obtained:

$$\frac{A}{h_0} = \frac{A_m}{1 + (A_D/dBn_c)(1/\mathsf{F}_0)}\mathsf{F}_0 \tag{7}$$

Equation (7) fits experimental data much better than Eq. (6). Within the range of present experimental conditions, the term $A_D/(dBn_c\mathsf{F}_0)$ is much greater than one; accordingly, Eq. (7) can be simplified to:

$$\frac{A}{h_0} = A_T dBn_c\mathsf{F}_0^2 \tag{8}$$

where $A_T = A_m/A_D$ is the only calibration factor. Interestingly, the above equation is very similar to Eq. (3), proposed by Zima and Ackermann (2002). Indeed, recalling that, within the framework of shallow water flow, the Strouhal and Froude numbers at resonance are related each other as $\mathsf{S_t}\,\mathsf{F}_0 = d/2B$, Eq. (3) can be rearranged to obtain Eq. (8) with $A_T = 9.02$. Interestingly, the value $A_T = 9.02$ is not much different from the values we found for the present experimental data.

For the secondary resonance condition we found $A_T = 12$ and $A_T = 11$ for the in-line and staggered configurations, respectively. With these values, Eq. (8) fits very well to experimental data for the in-line array, large flume, $n_c = 86.6\,m^{-2}$ and $n_c = 43.3\,m^{-2}$ (Fig. 7a) and for the staggered configuration, $n_c = 86.6\,m^{-2}$ and both the large and small flume (Fig. 7b). For the primary resonance condition we found that, with $A_T = 23$, Eq. (8) fits reasonably to data for both the in-line and staggered configurations and for the three densities, $n_c = 86.6\,m^{-2}$, $n_c = 43.3\,m^{-2}$ and $n_c = 28.9\,m^{-2}$ (Fig. 7c).

It is worth noting that for the higher cylinder density (i.e. $n_c = 86.6\,m^{-2}$), the scatter of experimental points about the theoretical solution is generally small, irrespective of cylinder pattern, flume arrangement and width, and resonance condition (primary or secondary). Conversely, amplitude data are somewhat uncertain when the cylinder density is $n_c = 43.3\,m^{-2}$ for both the secondary resonance (Fig. 7a) and the primary resonance (Fig. 7c). This is likely because the mechanisms promoting the vortex shedding synchronization over the whole cylinder array are not effective enough when the longitudinal spacing ratio is relatively large.

The overall comparison between computed and measured relative wave amplitude is anyway satisfactory (Fig. 7d). We remark that, as reported in Table 1, the model has been calibrated and validated for Froude numbers ranging between 0.10 and 0.19.

3.4 *The longitudinal wavelength of the metachronal wave*

Longitudinal wavelength was measured only when wave amplitude was large enough so that we could confidently, visually check that wavelength was not smaller than the distance between the ultrasonic water level sensors (i.e. approximately 2 m in the large flume and 0.7 m in the small flume). In addition, we considered only data for the first wave mode, since the few data measured for the second wave mode are not sufficiently reliable. Different length scales have been considered to scale the longitudinal wavelength (i.e. flow depth, cylinder diameter, flume width, transverse wavelength) and we found the flume width to be the most appropriate. However, this choice

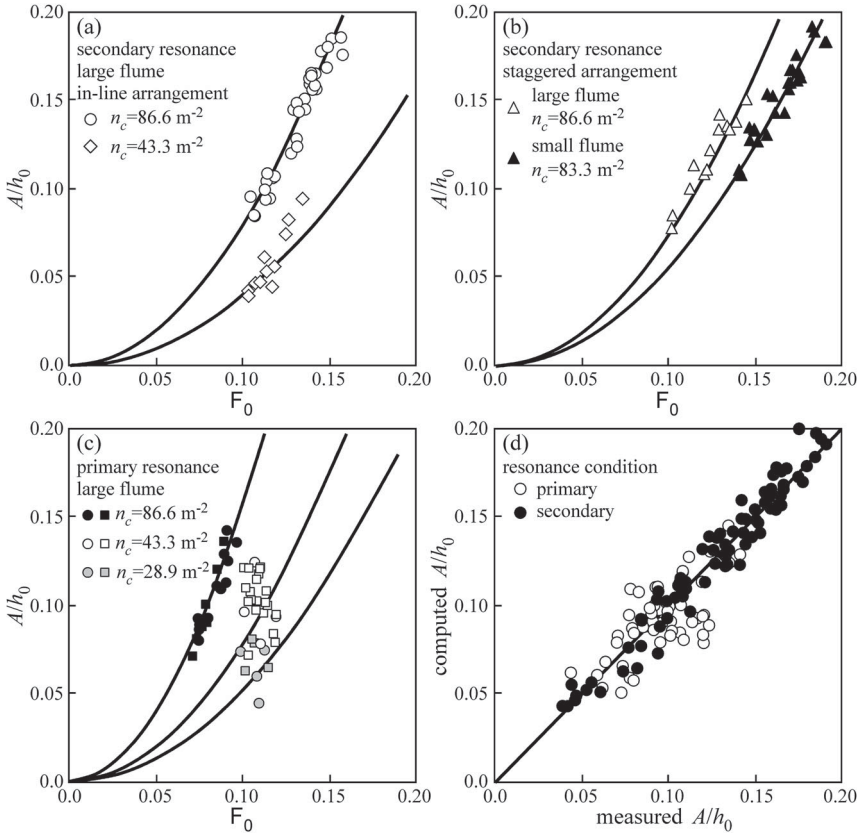

Figure 7 Panels (a), (b), and (c) show measured (symbols) and computed (lines) relative amplitude at resonance, A/h_0, as a function of the Froude number, F_0, using Eq. (8). (a) Secondary resonance condition in the large flume and in-line arrangement, for $n_c = 86.6\,\mathrm{m}^{-2}$ (circles) and $n_c = 43.3\,\mathrm{m}^{-2}$ (diamonds); (b) secondary resonance condition for $n_c = 86.6\,\mathrm{m}^{-2}$ and staggered arrangement in the large flume (white triangles) and in the small flume (black triangles); (c) primary resonance condition for $n_c = 86.6\,\mathrm{m}^{-2}$ (black symbols), $n_c = 43.3\,\mathrm{m}^{-2}$ (white symbols), and $n_c = 28.9\,\mathrm{m}^{-2}$ (grey symbols); circles and squares denote in-line and staggered arrangement, respectively; and (d) comparison between measured and computed relative wave amplitude at resonance; white and black symbols denote primary and secondary resonance condition, respectively. Only data measured by the innermost ultrasonic sensor (denoted by S_2 in Fig. 1) and for the first wave mode are plotted

is not robustly supported by the experimental data, since we considered only two different values of B.

Figure 8 shows the relative wavelength, λ/B, as it varies with the reduced velocity. Data cluster along two curves, for the primary and secondary resonance condition, irrespective of the cylinder arrangement and density. In both cases, wavelength reduces with U_r increasing. Interestingly, the decreasing behaviour of wavelength is not affected by the occurrence of resonance which, for $n = 1$, occurs at $U_r = 1/S_t = 4.9$ for the primary resonance condition, and $U_r = 6.25$–6.90 for the secondary resonance condition, depending on cylinder density and arrangement.

Data for the secondary resonance condition have a large scatter about the mean behaviour. This occurrence was rather surprising since the secondary resonance has the lower experimental uncertainties. Close inspection of data showed that, for the secondary resonance condition, relative wavelength is also dependent on flow rate (or water depth); the inset of Fig. 8 shows the different relative wavelength when flow rate is 6–8 l s^{-1} (white circles) and 18–20 l s^{-1} (black circles), with minor scatter about the interpolation curves.

Given the similar decreasing behaviour of wavelength with reduced velocity for the primary and secondary resonance condition, we scaled the reduced velocity with the theoretical value, U_{r0}, it assumes at resonance. This value can easily be computed, for each flow rate, by combining Eqs (1), (2) and (5), with $f_S = f_n$, and by using the appropriate Strouhal number. Figure 9 shows the relative wavelength, λ/B as it varies with the ratio U_r/U_{r0}. All points align along one curve. However, the scatter of points for the secondary resonance condition (white symbols in Fig. 9) is relatively large; this is likely because, as stated above, the reduced velocity is not the only parameter that controls wavelength in this case. More accurate data are needed, however, in order (i) to understand the reason for why a metachronal wave rather than a simple seiche is generated, and (ii) to find an equation to accurately predict the longitudinal wavelength. For the sake of completeness, Fig. 9 includes the few and rather uncertain data for the second mode, primary resonance (grey points). The result suggests that the longitudinal wavelength scales better with the channel width, irrespective of wave mode, than with the transverse wavelength (which is $2B$ for $n = 1$ and B for $n = 2$).

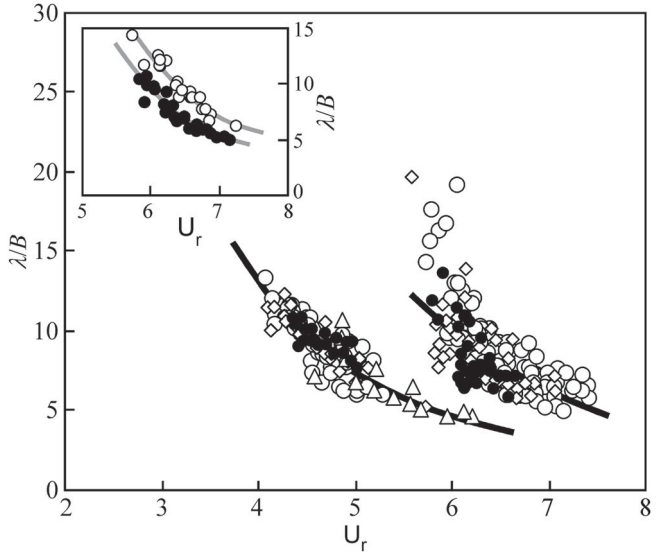

Figure 8 Relative longitudinal wavelength λ/B as a function of the reduced velocity. White symbols denote large flume data: $n_c = 86.6\,\mathrm{m}^{-2}$, in-line (circles) and staggered (diamonds) arrangement; $n_c = 43.3\,\mathrm{m}^{-2}$, in-line arrangement (triangles); black symbols denote small flume data: $n_c = 86.6\,\mathrm{m}^{-2}$ and staggered arrangement. The inset shows the relative wavelength at secondary resonance when flow rate is 6–8 $\mathrm{l\,s}^{-1}$ (white circles) and 18–20 $\mathrm{l\,s}^{-1}$ (black circles)

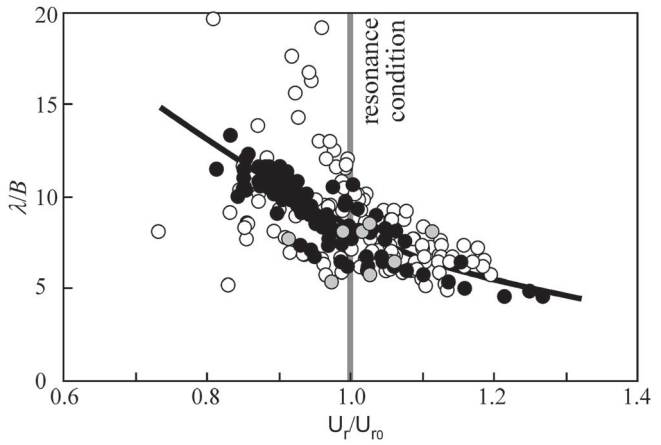

Figure 9 Relative longitudinal wavelength λ/B as a function of the relative reduced velocity, $\mathsf{U}_r/\mathsf{U}_{r0}$ for the first mode, primary (black circles) and secondary (white circles) resonance conditions, and second mode primary resonance condition (grey circles). The theoretical resonance condition is indicated by the vertical line at $\mathsf{U}_r/\mathsf{U}_{r0} = 1$

4 Conclusions

An extensive experimental investigation on the stationary waves that originate when an array of cylinders is placed in an otherwise uniform open channel flow was performed. On one hand, our experimental results confirmed previous findings. In particular we found that (i) the small-amplitude wave theory accurately predicts the natural oscillation frequency when the frequency is relatively small (i.e. smaller than 1.2–1.4 s^{-1} in the present experiments), whereas it tends to over-predict the actual frequency with frequency increasing, and (ii) the first mode, wave amplitude at resonance is fairly well predicted by Eq. (8). On the other hand, some new features of the phenomenon emerged from the experimental study. These are listed below.

(i) The standing wave produced by the periodic lift force associated with vortex shedding behind each cylinder of the array is a metachronal wave, rather than a pure transverse seiche.
(ii) Two resonance conditions for the first wave mode exist. The primary resonance condition occurs at a Strouhal number corresponding to that of an isolated cylinder ($\mathsf{S}_t \cong 0.2$ in the present experiments) and it is likely promoted by the upstream cylinders of the array; the secondary resonance condition, which is likely promoted by the inner cylinders, occurs at a smaller Strouhal number ($\mathsf{S}_t = 0.14$–0.16 in the present experiments).
(iii) The Strouhal number of the secondary resonance depends on the cylinder arrangement and density. It is larger for the staggered arrangement than for the in-line arrangement, and it decreases with increasing cylinder density.
(iv) The wave amplitude at the secondary resonance condition strongly depends on cylinder density. As the density is decreased by increasing the longitudinal spacing ratio, the wave amplitude decreases and, ultimately, reduces to zero.
(v) The longitudinal wavelength decreases over the reduced velocity range straddling the resonance condition from approximately (10–15) B to less than 5 B. The wavelength at resonance is on average eight times the flume width, B. However, the scatter of points about the average behaviour is large and the issue requires further specific investigation.

The existence of two resonance conditions for the first wave mode, which has never been reported in the literature on this issue, as well as the yet unclear mechanisms that make the first mode, secondary resonance oscillation prevail over the second mode, primary resonance oscillation, may be the reasons for the large scatter of data of previous experimental works. The experimental set-up used here was primarily designed to accurately measure the seiche amplitude and did not allow satisfactory investigation of the phenomena of which we were unaware, such as the dual resonance condition and the metachronal wave. Accordingly, the present results and discussion can be of help in designing future experiments aimed at improving our knowledge on the latter issues.

Notation

B = channel width (m)
d = cylinder diameter (m)
f_n = natural frequency (s^{-1})
f_S = Strouhal frequency (s^{-1})
f_v = actual vortex shedding frequency (s^{-1})
F = Froude number (–)
g = gravity acceleration ($\mathrm{m\,s}^{-2}$)

h_0 = mean flow depth (m)
k = longitudinal wavenumber (m^{-1})
L = length of the cylinder array in the flow direction (m)
m = transverse wavenumber (m^{-1})
n = seiche mode (–)
n_c = number of cylinders per unit horizontal area (m^{-2})
P = longitudinal spacing (m)
Q = flow rate ($l\ s^{-1}$)
R = Reynolds number (–)
s = cross-sectional area of a cylinder per unit horizontal area (–)
S_t = Strouhal number (–)
U = bulk flow velocity ($m\ s^{-1}$)
U_r = reduced velocity (–)
ν = kinematic viscosity of water ($1 \times 10^{-6}\ m^2\ s^{-1}$)

ORCiD

Daniele P. Viero http://orcid.org/0000-0003-0824-3990
Andrea Defina http://orcid.org/0000-0003-2907-8023

References

Alam, M. M., & Zhou, Y. (2008). Strouhal numbers, forces and flow structures around two tandem cylinders of different diameters. *Journal of Fluids and Structures*, *24*, 505–526. doi:10.1016/j.jfluidstructs.2007.10.001

Brennen, C., & Winet, H. (1977). Fluid mechanics of propulsion by cilia and flagella. *Annual Reviews of Fluid Mechanics*, *9*, 339–398. doi:10.1146/annurev.fl.09.010177.002011

Defina, A., & Pradella, I. (2014). Vortex-induced cross-flow seiching in cylinder arrays. *Advances in Water Resources*, *71*, 140–148. doi:10.1016/j.advwatres.2014.06.002

Falvey, H. T. (2003). Discussion of "Wave generation in open channels by vortex shedding from channel obstructions" by Laura Zima and Norbert Ackermann. *Journal of Hydraulic Engineering*, *129*, 919–919. doi:10.1061/(ASCE)0733-9429(2003)129:11(919)

Ghomeshi, M., Mortazavi-Dorcheh, S. A., & Falconer, R. (2007). Amplitude of wave formation by vortex shedding in open channels. *Journal of Applied Sciences*, *7*, 3927–3934. doi:10.3923/jas.2007.3927.3934

Hanko, Z. G. (1967). Vortex-induced oscillations at low-head weirs. *Journal of the Hydraulics Division*, *93*(6), 255–270.

Jafari, A., Ghomeshi, M., Bina, M., & Kashefipour, S. M. (2010). Experimental study on ten modes of transverse waves due to vertical cylinders in open channels. *Journal of Food, Agriculture and Environment*, *8*(2), 949–955.

King, R., & Johns, D. J. (1976). Wake interaction experiments with two flexible circular cylinders in flowing water. *Journal of Sound and Vibration*, *45*(2), 259–283. doi:10.1016/0022-460X(76)90601-5

Oengören, A., & Ziada, S. (1992). Vorticity shedding and acoustic resonance in an in-line tube bundle. Part II: Acoustic resonance. *Journal of Fluids and Structures*, *6*, 293–309. doi:10.1016/0889-9746(92)90011-Q

Oengören, A., & Ziada, S. (1998). An in-depth study of vortex shedding, acoustic resonance and turbulent forces in normal triangle tube arrays. *Journal of Fluids and Structures*, *12*, 717–758. doi:10.1006/jfls.1998.0162

Peruzzo, P., Defina, A., & Nepf, H. (2012). Capillary trapping of buoyant particles within regions of emergent vegetation. *Water Resources Research*, *48*, W07512. doi:10.1029/2012WR011944

Polak, D. R., & Weaver, D. S. (1995). Vortex shedding in normal triangular tube arrays. *Journal of Fluids and Structures*, *9*, 1–17. doi:10.1006/jfls.1995.1001

Rahmeyer, W., Robison, E., & Barfuss, S. L. (2010). *Physical modeling of wave oscillations from the I-84 Bridge Crossing of the New York Canal in Boise, Idaho* (UWRL Report – USU 686). Logan, UT: Utah Water Res. Lab., Utah State University.

Sarkar, A. (2012). Vortex-excited transverse surface waves in an array of randomly placed circular cylinders. *Journal of Hydraulic Engineering*, *138*, 610–618. doi:10.1061/(ASCE)HY.1943-7900.0000557

Schuster, J. C. (1967). *Canal capacity studies, Wave formation by bridge piers* (Hydraulics Branch Report HYD-485). Washington, DC: US Bureau of Reclamation.

Williamson, C. H. K., & Govardhan, R. (2004). Vortex-induced vibrations. *Annual Review of Fluid Mechanics*, *36*, 413–455. doi:10.1146/annurev.fluid.36.050802.122128

Williamson, C. H. K., & Govardhan, R. (2008). A brief review of recent results in vortex-induced vibrations. *Journal of Wind Engineering and Industrial Aerodynamics*, *96*, 713–735. doi:10.1016/j.jweia.2007.06.019

Zhao, K., Cheng, N.-S., & Huang, Z. (2014). Experimental study of free-surface fluctuations in open-channel flow in the presence of periodic cylinder arrays. *Journal of Hydraulic Research*, *52*(4), 465–475. doi:10.1080/00221686.2014.880858

Ziada, S., & Oengören, A. (1993). Vorticity shedding in an in-line tube bundle with large tube spacings. *Journal of Fluids and Structures*, *14*, 197–219. doi:10.1006/jfls.1993.1039

Ziada, S., & Oengören, A. (2000). Flow periodicity and acoustic resonance in parallel triangle tube bundles. *Journal of Fluids and Structures*, *7*, 661–687. doi:10.1006/jfls.1999.0259

Zima, L., & Ackermann, N. L. (2002). Wave generation in open channels by vortex shedding from channel obstructions. *Journal of Hydraulic Engineering*, *128*, 596–603. doi:10.1061/(ASCE)0733-9429(2002)128:6(596)